Diagnostic and intraoperative targeted molecular imaging for pancreatic cancer

Tummers, W.S.F.J.

Citation

Tummers, W. S. F. J. (2018, November 13). *Diagnostic and intraoperative targeted molecular imaging for pancreatic cancer*. Retrieved from https://hdl.handle.net/1887/66717

Cover Page

Universiteit Leiden

The handle http://hdl.handle.net/1887/66717 holds various files of this Leiden University dissertation.
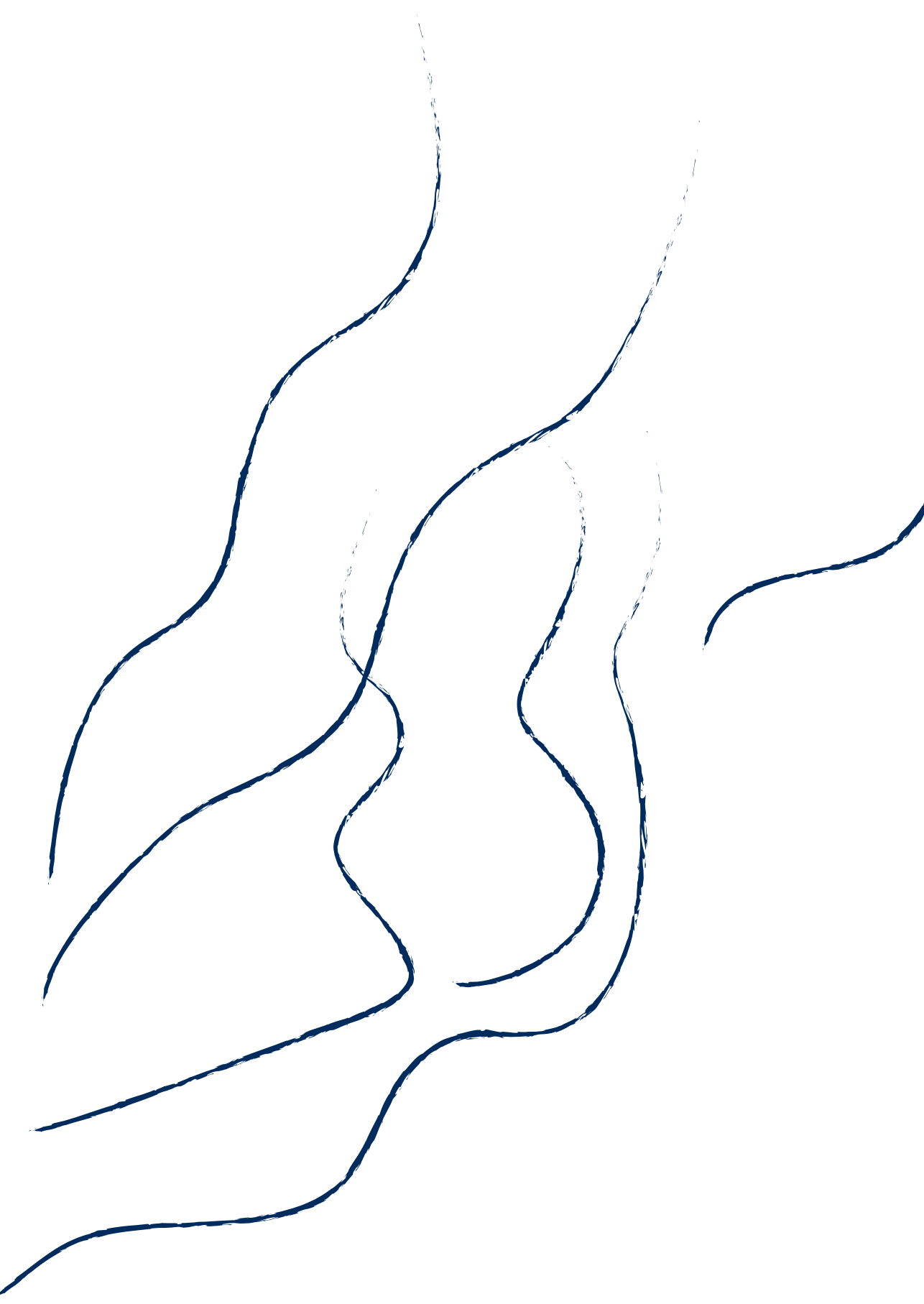
Author: Tummers, W.S.F.J.
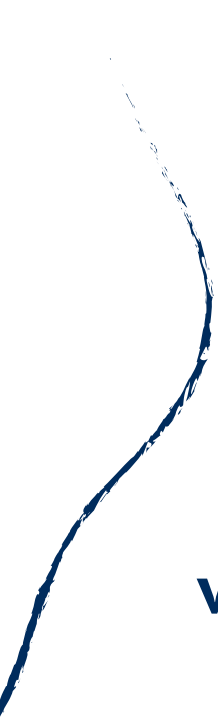**Title**: Diagnostic and intraoperative targeted molecular imaging for pancreatic cancer
Issue Date: 2018-11-13

Validation of Targeted Molecular Imaging for Pancreatic Cancer

Preclinical development and validation of multimodal probe for the tumor-specific imaging of pancreatic cancer

Tummers WS [1,2], Kimura RH [1], Abou-Elkacem L [1], Beinat C [1], Vahrmeijer AL [2], Swijnenburg RJ [2], Willmann JK [1], Gambhir SS [3]

[1] Department of Radiology, Molecular Imaging Program at Stanford (MIPS), Stanford University, Stanford, CA, 94305, USA. [2] Department of Surgery, Leiden University Medical Center, Albinusdreef 2, 2300 RC, Leiden, The Netherlands. [3] Departments of Radiology, Bioengineering, and Materials Science & Engineering, Molecular Imaging Program at Stanford. Canary Center at Stanford for Early Cancer Detection. Stanford University, Stanford, CA, 94305, USA.

ABSTRACT

Purpose: Intraoperative near-infrared fluorescence (NIRF) imaging could help stratification for the proper primary treatment for patients with pancreatic ductal adenocarcinoma (PDAC), and achieve complete resection since it allows visualization of cancer in real time. Integrin αvβ6, a target specific for PDAC, is present in >90% of patients, and is able to differentiate between pancreatitis and PDAC. A clinically translatable αvβ6-targeting NIRF agent was developed, based on a previously developed cysteine knottin peptide for PET imaging, R01-MG, and validated in preclinical mouse models.

Experimental Design: The applicability of the agent was tested for cell and tissue binding characteristics using cell-based plate assays, subcutaneous and orthotopic pancreatic models, and a transgenic mouse model of PDAC development (Pdx1-Cre$^{tg/+}$;KRas $^{LSL\ G12D/+}$;Ink4a/Arf$^{-/-}$). IRDye800CW was conjugated to R01-MG in a 1:1 ratio. R01-MG-IRDye800, was compared to a control peptide and IRDye800 alone.

Results: In subcutaneous tumor models a significantly higher tumor-to-background ratio (TBR) was seen in BxPC-3 tumors (2.5±0.1) compared to MiaPaCa-2 (1.2±0.1) (p<0.001), and to the control peptide (1.6±0.4) (p<0.005). In an orthotopic tumor model tumor-specific uptake of R01-MG-IRDye800 was shown compared to IRDye800 alone (TBR 2.7 versus 0.86). The fluorescent signal in tumors of transgenic mice was significantly higher, TBR of 3.6±0.94, compared to the normal pancreas of wild type controls, TBR of 1.0±0.17 (p<0.001).

Conclusion: R01-MG-IRDye800 shows specific targeting to αvβ6, and holds promise as a diagnostic and therapeutic tool to recognize PDAC for fluorescence-guided surgery. This agent can help improve the stratification of patients for a potentially curative, margin-negative resection.

INTRODUCTION

Pancreatic ductal adenocarcinoma (PDAC) has a dismal prognosis.[1, 2] In fact, it is the fourth leading cause of cancer-related deaths in the western world; 43,090 patients are estimated to die of PDAC in 2017 in the Unites States. The median size of a PDAC at the time of diagnosis is ~3.1cm, and this has not changed in the past three decades despite major advances in both anatomical and molecular imaging technologies as well as in vitro diagnostics.[3, 4] Early detection of pancreatic cancer is difficult because patients are often asymptomatic or present with non-specific symptoms until late stage disease.[4, 5] After diagnosis the patient selection for surgical resection is challenging. A potential curative resection can only be achieved in a minority of patients, and is dependent on tumor stage and grade. Two major predictors of long-term survival after resection are the achievement of tumor free resection margins and the absence of systemic metastases. Unfortunately, margin-positive resections (R1) are a frequent phenomenon (up to 70%) as is the emergence of distant metastases soon after surgery, which were likely present at the time of surgery in the form of visually occult micrometastases.[6-8] Failure to identify tumor-positive margins during surgery is not surprising, due to the tumor characteristics to quickly spread beyond the pancreas via perineural and perivascular pathways[9] and the inability of the surgeon to differentiate between tumor and (peritumoral) inflammatory tissue, such as associated chronic pancreatitis.[10, 11]

The integration of innovative molecular imaging techniques into the operating room can lead to the transformation of current gold standard intraoperative imaging modalities, such as intra-operative ultrasound and the surgeon's eyes, into pancreatic cancer-specific molecular imaging tools. Optical imaging in real-time, using a novel near-infrared fluorescent pancreatic cancer-targeting imaging agent, could add relevant information to the surgeon, by enhancing tumor margins and improving the detection of visually occult lesions. This would improve the selection of patients for the most suitable primary treatment.

In previous studies, out of a panel of different biomarkers, we selected integrin αvβ6 as the most promising target for pancreatic cancer detection, based on its potential to discriminate tumor and inflammation, to identify lymph node

05

metastases, to differentiate between viable tumor cells and necrosis in patients who received neoadjuvant therapy.[12, 13]

We previously developed a cysteine knottin that binds to integrin αvβ6 with subnanomolar affinity (Kd~1nM).[14] At this point, this peptide is tested in a Phase I trial in humans as a targeted PET tracer, [18F]FP-R01-MG-F2, without any safety concerns (eIND #126379). Zhang et al. recently published data showing the development and preclinical validation of R01 conjugated to the photoacoustic dye Atto-740.[15] Zhang showed selective binding of the imaging agent to αvβ6-positive tumors. However, this agent exhibited hepatobiliary clearance marked by high uptake in the liver, spleen, and intestine. For a pancreatic cancer imaging agent, a renal clearance pathway is preferred for a due to the close proximity of the liver, and therefore potential interference of signal. Since the PET tracer show renal clearance the fluorescent dye was changed to achieve
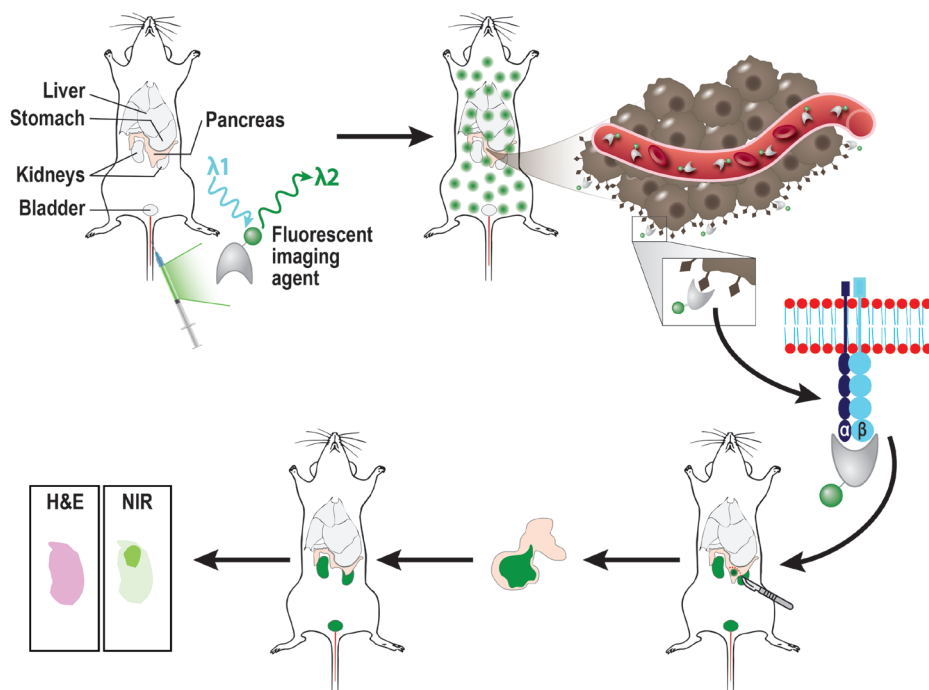

Figure 1. Schematic overview of imaging agent concept. Agent is injected intravenously, and migrates via the vessel to the target of interest (αvβ6). Resection of the pancreatic cancer can be performed guided by fluorescent signal, and fluorescent signal at microscopic level is conformed with tumor status on histopathology. The agent preferably has renal clearance, since fluorescent signal from the liver in case of a hepatic route could interfere with signal from the tumor.

these favorable pharmacokinetics. The NIR fluorescent dye IRDye800 is known to clear via the kidneys, and has a high extinction coefficient.[16] In addition, IRDye800 is already tested extensively in humans and shown safe in clinical studies.[11, 17] Therefore, IRDye800 was the NIR fluorescent dye of choice in the current study. The preferred imaging concept is shown in figure 1, highlighting the preference of an intravenously injected agent. This agent needs to bind selectively to the tumor receptors, facilitating fluorescence-guided resection, and excretion by the kidney's is favorable in pancreatic cancer surgery. Lastly, the fluorescent signal needs to be correlated to tumor status on H&E to ensure specific binding.

Here, we show the development and validation of a novel αvβ6-targeting probe for intraoperative tumor-specific fluorescent imaging of PDAC, with high potential for clinical translation.

05

MATERIALS AND METHODS

Materials and reagents
All Fmoc amino acids and Rink Amide resin were purchased from CS Bio Co. (Menlo Park, CA). Peptide synthesis were carried out following the standard solid phase Fmoc synthesis. Analysis and purification of the peptides was performed using the Dionex Summit high-performance liquid chromatography (HPLC) system (Dionex Corporation, Sunnyvale, CA) and reverse phase HPLC column Higins Analytical (Higins Analytical, Mountain View, CA) (C18, 4.6 mm × 250 mm). The mobile phase was 0.1% trifluoroacetic acid (TFA; Thermo Fisher Scientific, Pittsburgh, PA)) in water (solvent A) and 0.1% TFA in 90 % acetonitrile (CH3CN; Thermo Fisher Scientific, Pittsburgh, PA) in water (solvent B). Matrix assisted laser desorption/ionization time-of-flight mass spectrometry (MALDI-TOF MS) was performed by the Canary Center proteomics facility on AB Sciex 5800 TOF/TOF System (Foster City, CA).

Development of tumor-specific fluorescent probe
Knottin peptide R01-MG targeted integrin αvβ6 were synthesized using the described standard solid phase Fmoc synthesis, and folded and purified as previously described.[18] For labeling of the knottin peptide R01-MG, IRDye800

N-hydroxysuccinimide (NHS) ester (LI-COR Biosciences, Lincoln, Nebraska) was dissolved in anhydrous, amine-free dimethylformamide (DMF; Sigma Aldrich, St Louis, MO) to a 0.5 mg/ml solution. Knottin peptide R01-MG was dissolved in Dulbecco's Phosphate-Buffered Saline (DPBS; Life technologies, Foster City, CA) to a 1.5 mg/ml solution. IRDye800 NHS solution was mixed with knottin peptide R01 solution in 1:1 molar ratio. The reaction mixture was incubated and protected from light for up to 1 hour at room temperature. The reaction mixture was injected directly onto the HPLC column, and the separation of the product mixture followed using absorbance at 780 nm. The imaging agent had a retention time of 16.89 minutes and m/z of 4817. The lyophilized IRDye800-peptide was dissolved in 100uL dimethyl sulfoxide (DMSO; Thermo Fisher Scientific, Pittsburgh, PA) and 100uL DPBS. Maximum absorption wavelength of R01-MG-IRDye800 agent was performed using Cary50 (Varian).

Development of control cysteine knottin
The tumor-specific probe is based on the trypsin inhibitor, momordica cochinchinensis trypsin inhibitor (MCoTI-II). For the control cysteine knottin the binding sequence of R01-MG to $\alpha v \beta 6$ was replaced with the MCoTI-II sequence at these positions, to develop a control knottin most similar to the original R01-MG. This resulted in the following sequence; N'-GCPRILMRCRRDSDCPGACICRGNGYCG. Synthesis, folding and purification was performed as described. The control cysteine knottin had a retention time of 20.60 minutes and m/z of 3033. The control peptide was labeled with IRDye800 N-hydroxysuccinimide (NHS) ester (LI-COR Biosciences, Lincoln, Nebraska, USA) in a similar fashion as R01-MG-IRDye800. The reaction mixture was injected directly onto the HPLC column, and the separation of the product mixture followed using absorbance at 780 nm. The imaging agent had a retention time of 16.53 minutes.

Photostability
100 μL of R01-MG-IRDye800 (0.5×10^{-6} M) was placed in a 96-well plate in the SpectraMax Gemini EM microplate reader (Molecular Devices, Ramsey, MN, USA) in triplicate and scanned with laser light using maximum absorption wavelength (750 nm) and emission wavelength (800nm) for 30 min. Photobleaching was determined by the change in fluorescent intensity over time.

Human cancer cell lines

A total of six cancer cell lines were used for the cell-based experiments, including four pancreatic cancer cell lines (BxPC-3, BxPC-3-luc2, MiaPaCa-2, and AsPC-1), one colorectal cancer cell line (HCT-116), and one epidermoid carcinoma (A431). All cell lines, except for BxPC-3-luc2, were purchased from American Type Culture Collection (ATCC, Manassas, VA) and expression was authenticated within 6 months before the in vitro experiments. The BxPC-3-luc2 cell line was purchased from PerkinElmer (MA). BxPC-3 (CRL-1687TM), provided by ATCC, was used as source for the parental cell line. BxPC-3 and BxPC-3-luc2 cells were cultured in RPMI-1640 medium containing 10% fetal bovine serum, 1 % penicillin and streptomycin. MiaPaCa-2, HCT-116 and A431 cells were cultured in DMEM containing 10% fetal bovine serum, 1 % penicillin and streptomycin. For MiaPaCa-2 cells, also 2.5% horse serum was added according to ATCC guidelines.

05

Mouse cancer cell lines

The binding of R01-MG-IRDye800 to mouse αvβ6 was assessed to determine the *in vivo* specific binding to mouse αvβ6. The following two cell lines were used; a mouse breast cancer cell line (4T1), and mouse colon carcinoma cell line (CT-26). All cell lines were purchased from American Type Culture Collection (ATCC, Manassas, VA) and expression was authenticated within 6 months before the in vitro experiments. A maximum of ten passages was performed for all cells, between thawing and use in the described experiments. CT-26 cells were cultured in DMEM medium containing 10% fetal bovine serum, 1 % penicillin and streptomycin. 4T1 cells were cultured in RPMI-1640 medium containing 10% fetal bovine serum, 1 % penicillin and streptomycin.

Flow cytometry

All cells were tested for αvβ6 expression using flow cytometry. The cells were grown to 90% confluence and detached with trypsin/EDTA. After evaluation of cell viability using trypan blue, cells were adjusted to 1×10^6 per tube in ice-cold PBS with 4% formaldehyde for fixation and incubated in a binding buffer containing DMEM, 0.1% BDA and 0.1% NaN3 with 100ul of anti-αvβ6 mouse monoclonal antibody (10D5, ab77906, Abcam, Cambridge, United Kingdom) for 1h at room temperature. After incubation, cells were washed thrice and incubated with the secondary antibody anti-mouse IgG F(ab)$_2$ fragment

conjugated to Alexa Fluor® 647 (#4410, Cell Signaling Technology, Danvers, MA, United States, 1/800) for 30 min. After three washing steps with the washing buffer, cells were resuspended in 500ul PBS. Samples were measured on the Scanford flow cytometer (Custom Stanford and Cytek upgraded FACScan Analyzer) and 1×10^5 cells were counted.

Cell binding study

Human cancer cell lines BxPC-3 (αvβ6 positive) and MiaPaCa-2 (αvβ6-negative), and murine cancer cell lines 4T1 (αvβ6 positive) and CT-26 (αvβ6-negative) were placed in a 8 well chamberslide (0.7 cm^2, Nunc™ Lab-Tek™ II Chamber Slide™ System; ThermoFisher Scientific, Waltham, MA, USA) and grown to ~85% confluence. Cells were fixed for 20 min at 4 °C with 1% formaldehyde. R01-MG-IRDye800 was diluted in integrin-binding buffer (IBB). The IBB was similar as previously described [19], and added to the chamberslide with concentration of 0.1 µM, 0.2 µM or 0.5 µM and incubated at room temperature for 2 h. After being washed with DPBS three times, the chamber was removed and the nuclei were counter stained with ProLong® Gold Antifade Mountant with DAPI (ThermoFisher Scientific, MA, Waltham, USA). The cellular binding of R01-MG-IRDye800 was assessed by co-staining of cells with DAPI and fluorescence with the EVOS Cell Imaging Systems (EVOS FL Cell Imaging System, ThermoFisher Scientific, MA, USA) with EVOS light cube Cy7, excitation 710-740 and emission: 775-746, and EVOS light cube DAPI, excitation: 357-344 and emission: 447-460. For quantitative analysis, mean fluorescent intensity (MFI), defined as total counts/region of interest (ROI) pixel area, was calculated using custom ROI generated for each specimen using the imaging software ImageJ version 1.50i and bundled with 64-bit Java for Windows (National Institutes of Health, Bethesda, MD; http://rsb.info.nih.gov/nih-image). Specificity of the binding was determined by a blocking experiment with incubation of BxPC-3-luc2 cells with 0.5 µM of R01-MG-IRDye800 and varying amounts of R01-MG (50x (25 µM) – 150x (75 µM) – 200x (100 µM) excess), and by incubation of BxPC-3-luc2 cells with IRDye800 0.5 µM alone. All samples were done in triplicates. For IRDye800 alone, IRDye800-NHS ester was used which is equal to the dye used in the agent. The NHS ester was reacted with water before injection, to ensure no reaction with amine groups could take place. A linear regression analysis was performed to determine if there was a linear correlation between concentration

and fluorescent signal; for BxPC-3 (Y = 118171*X + 11944) and for MiaPaCa-2 (Y = 23296*X + 9738).

To identify fluorescence intensity with increasing amount of αvβ6 receptors, an experiment was designed with both BxPC-3 and MiaPaCa-2 cells, in varying percentages; with the lowest amount of receptors in 100% MiaPaCa-2, and increasing amounts onwards; 20% BxPC-3 - 80% MiaPaCa-2, 40% BxPC-3 - 60% MiaPaCa-2, 60% BxPC-3 - 40% MiaPaCa-2, 80% BxPC-3 - 20% MiaPaCa-2, and 100% BxPC-3. The cells were incubated with 0.5 µM of R01-MG-IRDye800 for 2 h. Additional cell experiments were performed comparing R01-MG-IRDye800 to the newly synthesized control peptide. BxPC-3 cells were placed on a 8-well chamberslide, and after fixation incubated with both agents separately at concentration of 0.1 µM, 0.2 µM or 0.5 µM.

Fluorescent imaging of αvβ6 in Small Animal Models

Subcutaneous mouse model of human pancreatic cancer
The Administrative Panel on Laboratory Animal Care of Stanford University approved all procedures using laboratory animals. Eight week old nude female mice (n=20) (Charles River) were injected with 1 million BxPC-3-luc2, A431, or MiaPaCa-2-luc cells into the right shoulder. Mice bearing 0.4-0.8 cm tumors (n=8 BxPC-3-luc2, n=3 A431, n=4 MiaPaCa-2) for R01-MG-IRDye800, and n=5 for control cysteine knottin) were fluorescently imaged at 800 nm using a commercially fluorescent imaging system (The Pearl Impulse imaging platform (LI–COR Biosciences, Lincoln, NE). For each animal we first obtained pre-injection images at 800 nm. R01-MG-IRDye800 (30 µM), the control cysteine knottin (30 µM), or IRDye800 alone (30uM) was dissolved in 200 µL PBS (pH 7.4) and administered to mice via tail-vein injection. The data was acquired from 30 min up to 24h after the injection of the imaging agent.

Xenograft mouse model of human pancreatic cancer
Human AsPC1 pancreatic ductal adenocarcinoma cells (αvβ6 positive) (ATCC, Manassas, VA) were cultured to 70%–80% confluency. AsPC-1 cells were cultured in DMEM medium containing 10% fetal bovine serum, 1% penicillin and streptomycin. AsPC1 cells were suspended in culture medium and mixed 1:1 with Matrigel® (BD Biosciences, San Jose, CA) for orthotopic implantation. Sterile insulin syringes were loaded with the mixture and kept on ice until

05

orthotopic implantation. After midline laparotomy, the pancreas of nu/nu mice was exposed, and AsPC1 cells (total of 6×10^6 cells, dissolved in 25 μL Matrigel containing epidermal growth factor [0.7 ng/mL], insulin-like growth factor [16 ng/mL], and transforming growth factor−β [2.3 ng/mL]; BD Biosciences, San Jose, CA) were co-injected into the body or tail of the pancreas in 8 female nude mice (6−8 weeks old; Charles River, Wilmington, MA). The abdomen was then closed by layers. Orthotopic xenografts were allowed to grow for 21 days. R01-MG-IRDye800 (30 μM) or IRDye800 (30 μM) was dissolved in 200 μL PBS (pH 7.4) and administered to mice via tail-vein injection. The data was acquired from 30 min up to 24h after the injection of the imaging agent.

Transgenic Mouse Model of PDAC
The transgenic pancreatic cancer mouse model (Pdx1-Cretg/+; KRasLSL G12D/+; Ink4a/Arf−/−) was used (n = 10), which spontaneously develops foci of pancreatic cancer within 4−7 weeks of age.[20] Tumor diameters ranged between 3.0 and 4.8 mm. Age-matched littermates without KRas[G12D] mutation were used as normal wildtype control (n = 10). R01-MG-IRDye800 (30 μM) was dissolved in 200 μL PBS (pH 7.4) and administered to mice via tail-vein injection, in both the wildtype controls and tumor-bearing mice.

Toxicity of R01-MG-IRDye800 in mice
The toxicity of R01-MG-IRDye800 in living mice was determined in Nu/Nu mice (n=3). After injection of R01-MG-IRDye800 (30 μM) the mice were followed for three weeks and weight and overall appearance was assessed. In addition, blood draws were done to assess effect on red and white blood cells, aspartate transaminase (ASAT), alanine transaminase (ALAT) and creatinine.

Ex vivo imaging and biodistribution
All the mice were sacrificed between 6 or 24 h postinjection of the imaging agent as described above. Optical imaging of the excised organs was carried out using The Pearl Impulse imaging platform at 800 nm for biodistribution studies.

NIR-fluorescent animal imaging analysis
The Pearl Impulse small animal imaging system (LI-COR) was used for NIR-fluorescence measurements to measure NIR-fluorescent signals of the tumor, biodistribution analysis and to calculate TBR (tumor-to-background ratios).

The specific and control images were normalized and regions of interest were marked. The background signals were extracted from the surrounding tissue that was defined as the (normal) tissue/organ that lies around the tumor. After measuring the signal intensity from the macroscopic images they were divided by each other using the following formula: TBR = mean signal tumor/ mean signal surrounding tissue.

Histology

Formalin-fixed paraffin-embedded tumor tissues were sectioned at 5 μm thickness and fluorescence imaging was performed using the Odyssey NIR scanner (LI-COR Biosciences). All histologic sections were stained with standard hematoxylin-eosin immunohistochemical staining (H&E). To confirm the presence of αvβ6, additional sections were stained with immunohistochemistry (IHC) for anti-human αvβ6 (1/80, 6.2A1, Biogen Idec, Cambridge, MA). For preparation of IHC staining, the slides were deparaffinized with xylene and rehydrated in serially diluted ethanol solutions (100%-50%), followed by demineralized water according to standard protocols. Endogenous peroxidase activity was blocked by incubation in 0.3% hydrogen peroxidase in phosphate buffered saline (PBS) for 20 min. Antigen retrieval for αvβ6 was performed with 0.4% pepsin incubation (Dako) at 37°C for 10 min. Following antigen retrieval, the tissue sections were incubated overnight with the primary antibodies in 100 μl for standard tissue sections at room temperature. The slides were washed with PBS, followed by incubation with secondary antibody at room temperature according to the Vectastain ABC HRP kit (Peroxidase, Mouse IgG, Vector Laboratories Inc., Burlingame, CA). After additional washing, the staining was visualized with 3,3-diaminobenzidine tetrahydrochloride solution (DAKO, Glustrup, Denmark) at room temperature for 5 minutes and counterstained with hematoxylin for 20 seconds. Finally, the tissue sections were dehydrated and mounted in Pertex (Histolab, Rockville, MD, USA).

Statistical Analysis

Analyses were performed in SPSS 22.0 (IBM technologies). All data were presented as the mean ± standard deviations. Means were compared using Independent-Samples T test, or with One-way ANOVA with post-hoc Bonferroni correction. A P-value of less than .05 was considered to indicate a significant

difference. Graphs and linear regression were performed in GraphPad Prism 7.0 (version 7.02, IBM Corp.)

RESULTS

IRDye800 (NIRF dye) conjugation of the cysteine knottins

R01-MG was synthesized, and labeled with IRDye800CW at 1:1 ratio (Figure S1A). In addition the control cysteine knottin was synthesized (Figure S1B), and conjugated following the same protocol. R01-MG-IRDye800 showed high stability without clear decrease in fluorescent signal after laser exposure at 750nm for 30 minutes (Figure S1C). This correlates to the stability of IRDye800 alone.[21]

αvβ6 expression on cancer cell lines

The expression of αvβ6 in the cancer cell lines (listed above) was evaluated by flow cytometry using the monoclonal antibody, 10D5, and shown in the supplementary figures (Figure S2). Four of the cancer cell lines showed high αvβ6 expression; BxPC-3-luc2, A431, AsPC-1 and 4T1. Three cancer cell lines showed none or low αvβ6 expression; MiaPaCa-2, HCT-116, CT-26. Based on these experiments, we selected BxPC-3 and A431 as positive and MiaPaCa-2 as negative controls respectively for further studies.

R01-MG-IRDye800 specificity

The retained αvβ6-specificity of R01-MG-IRDye800 was confirmed using chamberslide assays. An increase in agent concentration resulted in an almost linear increase in signal intensity in the αvβ6 positive cell line (BxPC-3), while the αvβ6 negative cell line (MiaPaCa-2) showed limited signal intensity (Figure 2A). The difference between the cell lines was observed for all the different concentration tested, however staining at the lowest concentration [0.1uM] was also weak in BxPC-3 cells (Figure 2A). Competition of R01-MG-IRDye800 with unlabeled R01-MG resulted in a 77.2% reduction in NIR signal intensity, suggesting that the αvβ6-specific binding capacity of R01-MG after conjugation to IRDye800 remained. In addition, in a cell assay with different concentration of αvβ6 receptors, simulated by different percentages of BxPC-3 and MiaPaca-2
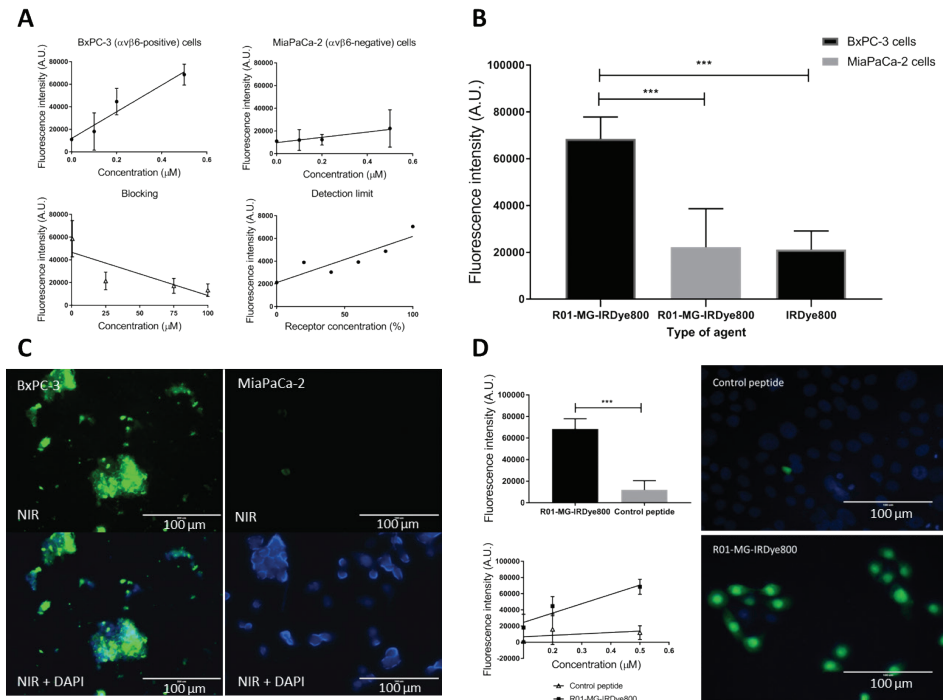
Figure 2. Cell binding study of R01-MG-IRDye800. (**A**) Graphic representation of fluorescent signal in BxPC-3 (αvβ6-positive), MiaPaCa-2 (αvβ6-negative) cells with regression line, after blocking with R01-MG, and with different concentrations of αvβ6-receptors. (**B**) Comparison of fluorescent signal in αvβ6-positive, and –negative cells after incubation with R01-MG-IRDye800, and after incubation with IRDye800 alone. (**C**) Representative fluorescence microscopy images of BxPC-3 cells with fluorescent signal at 800nm (green) and in overlay with DAPI signal (blue) to co-stain cell nuclei, and MiaPaCa-2 cells without any fluorescent signal at 800nm, but with DAPI-signal (blue). (**D**) Comparison between R01-MG-IRDye800 and newly synthesized fluorescent control knottin in BxPC-3 cells. ***; p<0.001, graphs are mean ± SD.

cells together, an increase in receptors led to a linear increase in fluorescent signal (R^2 = 0.80) (Figure 2A).

A significant difference in fluorescent (figure 2B, C) signal between BxPC-3 and MiaPaCa-2 cells was detected (p<0.001), and after 2h of incubation the fluorescent signal in BxPC-3 cells was 3.1 fold higher compared to the MiaPaca-2 cells. To control for non-specific staining of the fluorescent dye, incubation with the fluorescent dye alone, [0.5uM] IRDye800, was performed. The fluorescence intensity was 2.7 times lower compared to the incubation of [0.5uM] R01-MG-IRDye800 in BxPC-3 cells (p<0.001) and equal to the intensity in MiaPaCa-2 (p=1.000), indicating the specific binding of R01-MG-IRDye800 to αvβ6 (Figure

05

2B). A significant (p<0.001) lower fluorescent signal was observed after incubation with the control cysteine knottin, compared to R01-MG-IRDye800 as shown in Figure 2D. There was no fluorescent signal observed in both cell lines after incubation with PBS.

Mouse models

Specificity of R01-MG-IRDye800 in subcutaneous mouse models

To validate the performance of R01-MG-IRDye800 in living subjects, three different mouse models were used: (1) a subcutaneous model with different cell lines, (2)an orthotopic, intrapancreatic xenograftmodel using different cell lines, and (3) a spontaneous transgenic pancreatic cancer model. Subcutaneous tumor models were used to compare the binding of R01-MG-IRDye800 in αvβ6-positive and –negative tumors, and to determine the TBR over time (Figure 3A). The highest TBR for BxPC-3 mice was measured 20h post injection (4.08 ± 0.95) (Figure 3B). There was a difference in TBR between BxPC-3 tumors (2.5 ± 0.1), MiaPaCa-2 tumors (1.2 ± 0.1), and A431 tumors (1.8 ± 0.5), with a linear increase in TBR for both the BxPC-3 tumors and A431 tumors over time. The TBR of MiaPaCa-2 tumors remained stable at~1.0 during the investigated period of 5 hours (Figure 3C). BxPC-3 tumors had a significantly higher TBR compared to MiaPaCa-2 tumors (p<0.001) (Figure 3D). As controls R01-MG-IRDye800 was compared to a control peptide and fluorescent dye alone. The TBR of the mice injected with R01-MG-IRDye800 after 24h (3.5 ± 0.95) was significantly (p<0.005) higher compared to control peptide (1.6 ± 0.36), and dye alone (1.4 ± 0.2) (p<0.005) suggesting specific targeting of αvβ6 by R01-MG-IRDye800 (Figure 3E). In addition, compared to IRDye800 alone, a clear increase in mean TBR was seen over time for R01-MG-IRDye800, compared to an approximately constant mean TBR for IRDye800. This difference was significant from T=4h after injection (T=0h p=0.95, T=1h p=0.16, T=3h p=0.05, T=4h p<0.001, T=6h p<0.001, T=24h p<0.005) (Figure 3F).

αvβ6 binding and biodistribution in orthotopic mouse models

The efficacy of R01-MG-IRDye800 to bind and detect αvβ6 *in vivo* was evaluated in pancreatic cancer orthotopic xenografts implanted in nude mice. A mean TBR of 2.7 ± 1.22 at 24 hours post-injection was measured, compared to a mean TBR of 0.86 ± 0.13 for IRDye800 alone (Figure 4A). *Ex vivo* NIR-fluorescence measurements showed tumor specificity of the tracer with a mean TBR of 6.96 ±
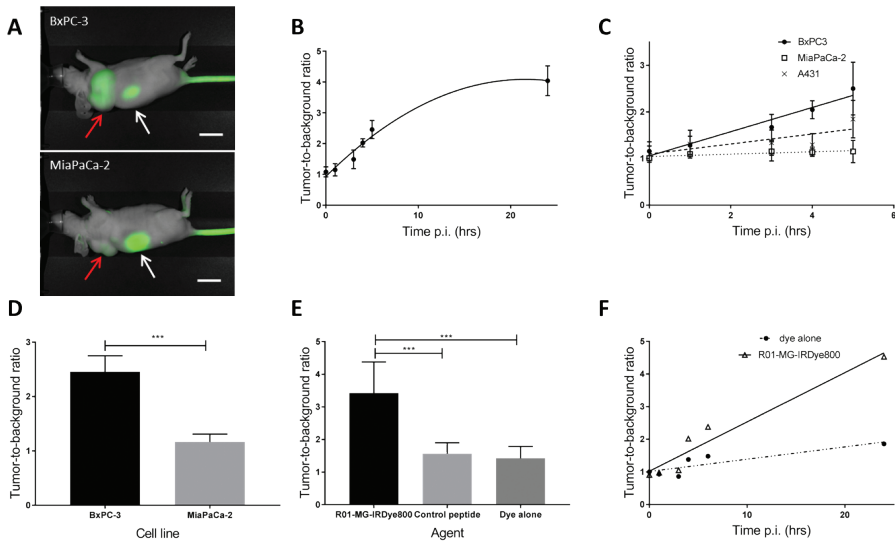
Figure 3. Preclinical validation R01-MG-IRDye800 in subcutaneous tumor models at 800nm. (**A**) Representative image of mouse with BxPC-3 and MiaPaCa-2 tumor 4h post-injection of R01-MG-IRDye800, and clear excretion via de kidneys. The tumor is indicated with a red arrow, the kidneys with white arrow. (**B**) Tumor-to-background ratio over time in BxPC-3 tumors with nonlinear fit curve, and (**C**) in tumors with different levels of αvβ6. (**D**) Comparison of maximum TBR in BxPC-3 and MiaPaCa-2 tumors, 5h post injection. (**E**) Validation of αvβ6-specific binding with R01-MG-IRDye800 compared to a control cysteine knottin and the fluorescent dye alone at maximum TBR, and (**F**) over time. Scale bar represent 1 cm. Graphs are mean ± SD.
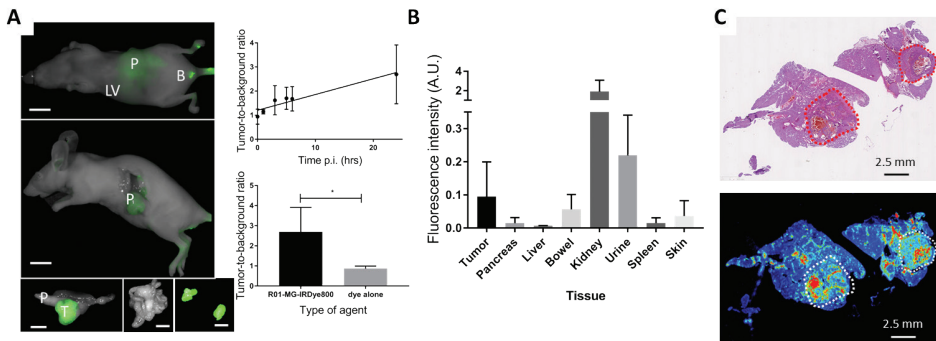
Figure 4. Validation in pancreatic cancer orthotopic xenografts at 800nm. (**A**) Representative images of tumor visualization using R01-MG-IRDye800, both in vivo and ex vivo. Ex vivo the pancreas with tumor is shown (left), the bowel (middle), and the kidney's (right). TBR in vivo over time, and comparison of maximum TBR between R01-MG-IRDye800 and IRDye800 alone. (**B**). Biodistribution of R01-MG-IRDye800, with highest uptake in the kidneys. (**C**) Correlation between tumor on H&E (outlined in red), and increased fluorescent signal. Scale bar represent 1 cm, unless indicated differently. P = pancreas, B = bladder, LV = liver. Graphs are mean ± SD.

2.2. Biodistribution assays showed high fluorescence in the kidneys (MFI 1.12 AU) and urine (MFI 0.22 AU) compared to the liver (MFI 0.007 AU) indicating a renal clearance route, and some fluorescence in the bowel (MFI 0.03 AU) and skin (MFI 0.02 AU) (Figure 4B). Fluorescence in the bowel can be explained by mild αvβ6 expression in gastro-intestinal tract mucosa.[22, 23] At the microscopic level, high fluorescence matched well with location of the tumor on H&E (Figure 4C).

Validation in transgenic mouse models

In the spontaneous transgenic tumor mouse model, the tumor could be visualized, even with the skin intact, and fluorescence localized at tumor regions was clearly visible *ex vivo* (Figure 5A). Even a subcentimeter metastasic lesion on the bowel (0.7 x 0.5 cm) could be visualized with fluorescence, corresponding to tumor-positive H&E (Figure 5B). In mice with the tumor genotype, the TBR
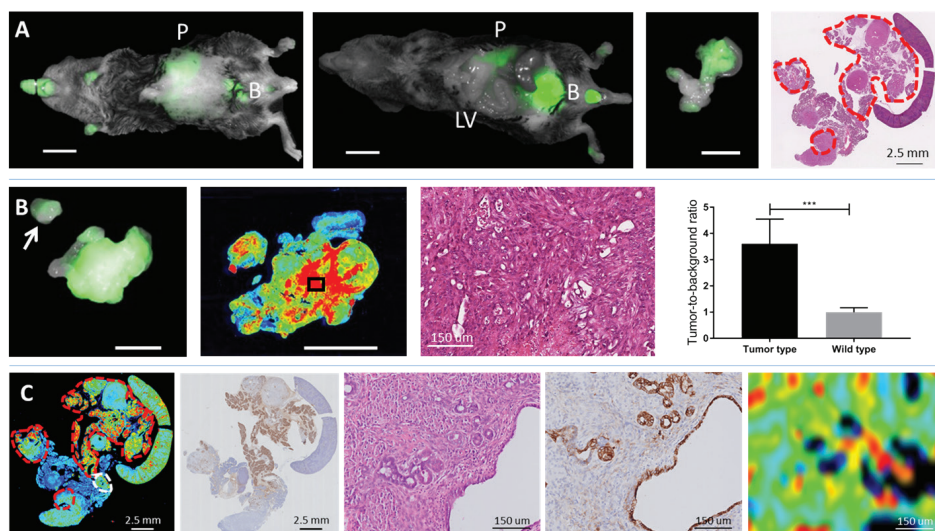

Figure 5. Fluorescent imaging and validation of R01-MG-IRDye800 in transgenic mice model at 800nm. (**A**) In vivo fluorescent imaging of mouse with pancreatic cancer, showing agent excretion via the kidneys in mouse with skin and without skin. In addition, ex vivo fluorescent imaging of resected pancreas with localized fluorescence and corresponding H&E section of entire pancreas with tumor localizations (outlined in red). (**B**) Ex vivo fluorescent imaging of primary tumor with subcentimeter metastasis on the bowel (white arrow), and corresponding fluorescence intensity scan with Odyssey Imaging System (LI-COR) showing high fluorescence in tumor areas, with corresponding H&E section of PDAC (black box). In addition, a graphic representation of mean TBR in transgenic mice of tumor versus normal pancreas (p<0.001). (**C**) Immunohistochemical correlation between fluorescent signal, tumor status and αvβ6 expression. Scale bar represent 1 cm, unless indicated differently. P = pancreas, B = bladder, LV = liver. Graphs are mean ± SD.

obtained with R01-MG-IRDye800 (3.6 ± 0.94) was significantly higher compared to the TBR in the normal pancreas of the WT controls after R01-MG-IRDye800 infusion (1.0 ± 0.17) (p<0.001) (Figure 5B). Fluorescent signal, and tumor status corresponded well to αvβ6 expression as assessed by immunohistochemistry (Figure 5C). To resemble the human situation, fluorescent signal provided by R01-MG-IRDye800 showed successful distinction between PDAC and peritumoral inflammation when in close proximity, even on microscopic level (Figure S3).

Toxicity of R01-MG-IRDye800

Pilot toxicity of the agent was determined in nude mice (N=3) by measurement of weight and hematology and chemistry blood panels. There was no significant difference observed in weight of mice pre-injection of R01-MG-IRDye800, directly after injection (p=0.054) and after the observation period of 3 weeks (p=0.732). The liver panel slightly increased after agent injection, and red blood cells count decreased, but all returned to baseline levels after follow-up. A slight increase in white blood cell count and creatinine was also seen, but these levels remained within normal limits for the entire observation period (Figure S4).

05

DISCUSSION

To improve the dismal prognosis of patients with PDAC, focus should be on early detection, improved patient selection for treatment and better surgical outcomes. A significant number of patients with PDAC present while the disease has already spread and will therefore not benefit from surgery as primary treatment. A limitation of conventional imaging techniques, such as CT and MRI, is the low sensitivity for detection of subcentimeter lesions and therefore metastatic spread is not always detected prior to surgery.[24] To overcome this limitation, optical imaging could be an additional tool to be applied during a diagnostic laparoscopy, prior to resection, to screen the abdomen for potential metastatic spread, such as liver or peritoneal metastases. For superficial lesions, fluorescent imaging is superior. Adjacent to that, for a more thorough screening of the liver, optoacoustic imaging could be added to provide sufficient depth penetration.[10, 25] If no spread is found in this initial stage, the surgery can proceed using the same optical imaging techniques to guide the resection. During resection, use of optical imaging can improve radical resection rates

by enhancing tumor margins and increase detection of tumor-positive lymph nodes.[26]

Previously, Hutteman et al. showed the use of the non-targeted optical imaging agent, Indocyanine Green (ICG), for the detection of PDAC. It was concluded that no useful tumor demarcation could be visualized after intravenous injection of ICG. However, the common bile duct and biliary anastomoses were clearly visualized.[27] Clinical trials performed in other malignancies, such as ovarian cancer, using tumor-specific imaging agents, showed successful use of this technique for the specific identification of cancer during surgery.[11, 28-30]

Integrin αvβ6 has been shown to be a promising target for identification of PDAC, and differentiation with pancreatitis and normal pancreatic tissue, with retained expression in vital tumor cells after neoadjuvant therapy.[12, 13, 15, 31, 32] Nowadays, the majority of patients will receive neoadjuvant therapy prior to surgery due to late onset of symptoms and therefore, presentation with locally advanced disease, or borderline resectable tumors. Currently, the distinction after neoadjuvant therapy between necrosis, fibrosis and vital tumor is impossible using conventional imaging techniques, and tumor-specific imaging could potentially fill this gap and be of added value in the diagnostic process.

Cysteine knottin peptides are relatively small (3-4 kDa), and have been extensively validated as alternative molecular imaging agents to antibodies.[31, 33, 34] We showed that the previously engineered cysteine knottin peptide R01-MG[18] demonstrated high and specific tumor uptake and high tumor-to-normal tissue ratios in mouse models of integrin αvβ6-positive PDAC, after conjugation to the near-infrared fluorescent dye, IRDye800. Moreover, the agent did not accumulate in integrin αvβ6-negative tumors. Due to the well-defined secondary structure, cysteine knottin peptides possess improved *in vivo* stability, and resist both chemical and physical insult compared to linear peptides, such as "A20".[18, 35-37] R01-MG-IRDye800 targets integrin αvβ6 with high affinity binding (Kd = 1.2 nM) and in a highly specific manner,[18] compared to for example cyclic-RGD, which mainly targets αvβ3, but also αvβ5, α5β1, α6β4, α4β1, and αvβ6.[38]

To prove that R01-MG-IRDye800 specifically targets αvβ6, and fluorescent signal in the tumor is not due to enhanced permeability and retention (EPR)

effect, especially seen in subcutaneous tumor models,[39] we have chosen to use a humanized transgenic mouse model. In addition, we performed several control studies using IRDye800 alone, and a newly synthesized control peptide with similar characteristics as the targeting peptide. Furthermore, to minimize non-specific leakage of the agent to the tumor, subcutaneous tumors with BxPC-3 cells were used which are known to be poorly leaky tumors, and therefore minimize EPR effect.[40] Our studies showed that the fluorescent signal of R01-MG-IRDye800 was significantly higher compared to both controls, indicating specific binding of R01-MG-IRDye800 to $\alpha v\beta 6$.

A limitation of using optical imaging as described here, is the use of one target to image the tissue of interest compared to multiplexing, targeting of multiple markers, to increase the detection sensitivity and potentially assess aggressiveness of the tumor.[41] Ideally, you would be able to deliver a cocktail of imaging agents to patients, each targeting a specific biomarker that is known to be overexpressed in PDAC and supplement each other for improved detection.[13] However, at this point none of the newly developed NIR tumor-specific optical imaging agents is approved by the U.S. Food and Drug Administration (FDA), which is partly due to the comprehensive process and costs associated with getting regulatory approval for an optical imaging agent, and the current lack of proven patient benefit.[42] Therefore, the possibility to deliver multiple agents at once, can probably not be realized in the near future. A benefit of the investigated target is that $\alpha v\beta 6$ is overexpressed in > 95% of PDAC patients, and significantly higher expressed in PDAC versus pancreatitis and normal pancreatic tissue.[13] Therefore, it is expected that multiplexing will not cause significant benefits over the use of R01-MG-IRDye800 as a single agent. As reported above, the differentiation between chronic pancreatitis and PDAC is one of the aspects where tumor-specific molecular imaging can be of additional benefit to the patient. A limitation of this study is that the agent is not tested in chronic pancreatitis mouse models. However, we know from previous performed research that $\alpha v\beta 6$ expression is significantly lower in pancreatitis compared to PDAC.[12, 13] In addition, we did address the difference in fluorescent signal between PDAC and peritumoral inflammation, because if the technique is able to do this, it would fill a clinically relevant gap in conventional imaging techniques. Based on our results, and due to high specific binding of the agent,

05

no limitations are expected for the clinical use of this agent for tumor-specific detection.

Our developed agent has high potential for clinical translation into patients, since it consists of two parts that are already successfully translated into humans. The cysteine knot peptide, R01-MG, is currently used in the clinic as an αvβ6-targeting PET tracer for the detection of pancreatic cancer (eIND #126379, NCT02683824) and the NIR fluorescent dye, IRDye800CW, has already been used for fluorescence-guided surgery in multiple clinical trials.[11, 30] We performed a pilot toxicology study that showed that the newly developed agent was well tolerated. However, some changes in hematology and chemistry blood panels were seen immediately after injection, which could potentially be due to the agent. These levels returned within the normal range after observation, but before final conclusions can be drawn, larger toxicology studies need to be performed to determine the meaning of these changes.

In conclusion, the developed optical imaging agent R01-MG-IRDye800 binds selectively to αvβ6. In cell studies, R01-MG-IRDye800 outperformed all controls, and a clear correlation between levels of receptor expression and fluorescence signal was found. In multiple preclinical mouse models, tumor-specific targeting was achieved, with favorable renal clearance. The agent exhibited high tumor-to-background ratios, and clear correlation between fluorescence signal and histopathologic evidence of PDAC. Thanks to the fact that this agent contains two elements, R01-MG and IRDye800 that were already proven to be safe for use in humans, we do not expect major hurdles for the clinical translation of this optical imaging agent.

ACKNOWLEDGMENTS.

REFERENCES

1. Jemal, A., et al., Cancer statistics, 2010. CA Cancer J Clin, 2010. 60(5): p. 277-300.

2. American Cancer Society, I. Key Statistics for Pancreatic Cancer. 2017 [cited 2017 July 31].

3. Laeseke, P.F., et al., Combining in Vitro Diagnostics with in Vivo Imaging for Earlier Detection of Pancreatic Ductal Adenocarcinoma: Challenges and Solutions. Radiology, 2015. 277(3): p. 644-61.

4. Tummala, P., O. Junaidi, and B. Agarwal, Imaging of pancreatic cancer: An overview. J Gastrointest Oncol, 2011. 2(3): p. 168-74.

5. Jang, J.Y., et al., A prospective randomized controlled study comparing outcomes of standard resection and extended resection, including dissection of the nerve plexus and various lymph nodes, in patients with pancreatic head cancer. Ann Surg, 2014. 259(4): p. 656-64.

6. Verbeke, C.S., Resection margins and R1 rates in pancreatic cancer--are we there yet? Histopathology, 2008. 52(7): p. 787-96.

7. Verbeke, C.S., et al., Redefining the R1 resection in pancreatic cancer. Br J Surg, 2006. 93(10): p. 1232-7.

8. Verbeek, F.P., et al., Image-guided hepatopancreatobiliary surgery using near-infrared fluorescent light. J Hepatobiliary Pancreat Sci, 2012. 19(6): p. 626-37.

9. Zhang, J.F., et al., Influence of perineural invasion on survival and recurrence in patients with resected pancreatic cancer. Asian Pac J Cancer Prev, 2013. 14(9): p. 5133-9.

10. Vahrmeijer, A.L., et al., Image-guided cancer surgery using near-infrared fluorescence. Nat Rev Clin Oncol, 2013. 10(9): p. 507-18.

11. Rosenthal, E.L., et al., Safety and Tumor-specificity of Cetuximab-IRDye800 for Surgical Navigation in Head and Neck Cancer. Clin Cancer Res, 2015.

12. de Geus, S.W., et al., Selecting Tumor-Specific Molecular Targets in Pancreatic Adenocarcinoma: Paving the Way for Image-Guided Pancreatic Surgery. Mol Imaging Biol, 2016.

13. Tummers WS, F.S.A., Boonstra MC, Prevoo HA, Sier CF, Mioeg JS, Morreau J, van Eijck C, Kuppen P, van de Velde CJ, Bonsing BA, Vahrmeijer AL, Swijnenburg RJ Selection of optimal molecular targets for tumor-specific imaging in pancreatic ductal adenocarcinoma. Oncotarget, 2017. May.

14. Kimura, R.H., et al., Pharmacokinetically stabilized cystine knot peptides that bind alpha-v-beta-6 integrin with single-digit nanomolar affinities for detection of pancreatic cancer. Clin Cancer Res, 2012. 18(3): p. 839-49.

15. Zhang, C., et al., A Cystine Knot Peptide Targeting Integrin alphavbeta6 for Photoacoustic and Fluorescence Imaging of Tumors in Living Subjects. J Nucl Med, 2016.

16. LI-COR Website. IRDye® 800CW NHS Ester Properties. 2016. Available from: https://www.licor.com/clinical_translation/irdye_800CW_NHS_ester_optical_properties_and_structure.html.

17. Lamberts, L.E., et al., Tumor-Specific Uptake of Fluorescent Bevacizumab-IRDye800CW Microdosing in Patients with Primary Breast Cancer: A Phase I Feasibility Study. Clin Cancer Res, 2017. 23(11): p. 2730-2741.

18. Kimura, R.H., et al., Pharmacokinetically stabilized cystine knot peptides that bind alpha-v-beta-6 integrin with single-digit nanomolar affinities for detection of pancreatic cancer. Clin Cancer Res, 2012. 18(3): p. 839-849.

19. Kimura, R.H., et al., Engineered cystine knot peptides that bind alphavbeta3, alphavbeta5, and alpha5beta1 integrins with low-nanomolar affinity. Proteins, 2009. 77(2): p. 359-69.

20. Aguirre, A.J., et al., Activated Kras and Ink4a/Arf deficiency cooperate to produce metastatic pancreatic ductal adenocarcinoma. Genes Dev, 2003. 17(24): p. 3112-26.

21. Peng X, D.D., Volcheck WM, Bashford GR, Lamb DT, Grone DL, Zhang Y, Johnson CM, Phthalocyanine dye as an extremely photostable and highly fluorescent near-infrared labeling reagent. Proc. SPIE 6097, Optical Molecular Probes for Biomedical Applications, 60970E 2006.

05

22. Knight, P.A., et al., Enteric expression of the integrin alpha(v)beta(6) is essential for nematode-induced mucosal mast cell hyperplasia and expression of the granule chymase, mouse mast cell protease-1. Am J Pathol, 2002. 161(3): p. 771-9.

23. Brown, J.K., et al., Integrin-alphavbeta6, a putative receptor for foot-and-mouth disease virus, is constitutively expressed in ruminant airways. J Histochem Cytochem, 2006. 54(7): p. 807-16.

24. Lee, Y.J., et al., Hepatocellular carcinoma: diagnostic performance of multidetector CT and MR imaging-a systematic review and meta-analysis. Radiology, 2015. 275(1): p. 97-109.

25. Zackrisson, S., S.M. van de Ven, and S.S. Gambhir, Light in and sound out: emerging translational strategies for photoacoustic imaging. Cancer Res, 2014. 74(4): p. 979-1004.

26. Hiroshima, Y., et al., Fluorescence-guided surgery, but not bright-light surgery, prevents local recurrence in a pancreatic cancer patient derived orthotopic xenograft (PDOX) model resistant to neoadjuvant chemotherapy (NAC). Pancreatology, 2015. 15(3): p. 295-301.

27. Hutteman, M., et al., Near-infrared fluorescence imaging in patients undergoing pancreaticoduodenectomy. Eur Surg Res, 2011. 47(2): p. 90-7.

28. Hoogstins, C.E., et al., A Novel Tumor-Specific Agent for Intraoperative Near-Infrared Fluorescence Imaging: A Translational Study in Healthy Volunteers and Patients with Ovarian Cancer. Clin Cancer Res, 2016. 22(12): p. 2929-38.

29. Burggraaf, J., et al., Detection of colorectal polyps in humans using an intravenously administered fluorescent peptide targeted against c-Met. Nat Med, 2015.

30. van Dam, G.M., et al., Intraoperative tumor-specific fluorescence imaging in ovarian cancer by folate receptor-alpha targeting: first in-human results. Nat Med, 2011. 17(10): p. 1315-9.

31. Kimura, R.H., et al., Pharmacokinetically stabilized cystine knot peptides that bind alpha-v-beta-6 integrin with single-digit nanomolar affinities for detection of pancreatic cancer. 2012(1078-0432 (Print)).

32. Hackel, B.J., et al., 18F-fluorobenzoate-labeled cystine knot peptides for PET imaging of integrin alphavbeta6. 2013(1535-5667 (Electronic)).

33. Moore, S.J. and J.R. Cochran, Engineering knottins as novel binding agents. Methods Enzymol, 2012. 503: p. 223-51.

34. Sarah J.Moore, C.L.L., Jennifer R.Cochran, Knottins: disulfide-bonded therapeutic and diagnostic peptides. Drug Discov Today Technol, 2012. 9(1): p. e1-e70.

35. Hausner, S.H., et al., Evaluation of an integrin alphavbeta6-specific peptide labeled with [18F]fluorine by copper-free, strain-promoted click chemistry. 2013(1872-9614 (Electronic)).

36. Hausner, S.H., et al., Use of a peptide derived from foot-and-mouth disease virus for the noninvasive imaging of human cancer: generation and evaluation of 4-[18F]fluorobenzoyl A20FMDV2 for in vivo imaging of integrin alphavbeta6 expression with positron emission tomography. 2007(0008-5472 (Print)).

37. Hausner, S.H., et al., Targeted in vivo imaging of integrin alphavbeta6 with an improved radiotracer and its relevance in a pancreatic tumor model. Cancer Research, 2009. 69(14): p. 5843-5850.

38. Shi, J., F. Wang, and S. Liu, Radiolabeled cyclic RGD peptides as radiotracers for tumor imaging. Biophys Rep, 2016. 2(1): p. 1-20.

39. Prabhakar, U., et al., Challenges and key considerations of the enhanced permeability and retention effect for nanomedicine drug delivery in oncology. Cancer Res, 2013. 73(8): p. 2412-7.

40. Kunjachan, S., et al., Passive versus active tumor targeting using RGD- and NGR-modified polymeric nanomedicines. Nano Lett, 2014. 14(2): p. 972-81.

41. Zheng, X., et al., Successively activatable ultrasensitive probe for imaging tumour acidity and hypoxia. 2017. 1: p. 0057.

42. Tummers, W.S., et al., Regulatory Aspects of Optical Methods and Exogenous Targets for Cancer Detection. Cancer Res, 2017. 77(9): p. 2197-2206.